Shaping organs by a wingless-int/Notch/nonmuscle myosin module which orients feather bud elongation

Ang Li[a], Meng Chen[b], Ting-Xin Jiang[a], Ping Wu[a], Qing Nie[b], Randall Widelitz[a], and Cheng-Ming Chuong[a,1]

[a]Department of Pathology, University of Southern California Keck School of Medicine, Los Angeles, CA 90033; and [b]Department of Mathematics, University of California, Irvine, CA 92697-3875

Edited by Neil H. Shubin, The University of Chicago, Chicago, IL, and approved March 8, 2013 (received for review November 14, 2012)

How organs are shaped to specific forms is a fundamental issue in developmental biology. To address this question, we used the repetitive, periodic pattern of feather morphogenesis on chicken skin as a model. Avian feathers within a single tract extend from dome-shaped primordia to thin conical structures with a common axis of orientation. From a systems biology perspective, the process is precise and robust. Using tissue transplantation assays, we demonstrate that a "zone of polarizing activity," localized in the posterior feather bud, is necessary and sufficient to mediate the directional elongation. This region contains a spatially well-defined nuclear β-catenin zone, which is induced by wingless-int (Wnt)7a protein diffusing in from posterior bud epithelium. Misexpressing nuclear β-catenin randomizes feather polarity. This dermal nuclear β-catenin zone, surrounded by *Notch1* positive dermal cells, induces *Jagged1*. Inhibition of Notch signaling disrupts the spatial configuration of the nuclear β-catenin zone and leads to randomized feather polarity. Mathematical modeling predicts that lateral inhibition, mediated by Notch signaling, functions to reduce Wnt7a gradient variations and fluctuations to form the sharp boundary observed for the dermal β-catenin zone. This zone is also enriched for nonmuscle myosin IIB. Suppressing nonmuscle myosin IIB disrupts directional cell rearrangements and abolishes feather bud elongation. These data suggest that a unique molecular module involving chemical–mechanical coupling converts a pliable chemical gradient to a precise domain, ready for subsequent mechanical action, thus defining the position, boundary, and duration of localized morphogenetic activity that molds the shape of growing organs.

anterior–posterior axial orientation | boundary formation | denoising | morphogen gradient

During their morphogenesis, each organ must be oriented and shaped properly. To achieve this, progenitor cells in organ primordia are guided to coordinated orientation and self-regulated size and shape by tissue interactions (1). We have proposed a general scheme where multiple localized activity modules in organ primordia can serve as the foundation to generate complex patterns and shapes (2). Different cellular activity modules can be based on highly localized physical processes such as cell polarity, rearrangement, proliferation, apoptosis, and differentiation. The number, size, position, duration, and spacing of these activity modules can converge to form a spectrum of organ designs suitable for different physiological stages or adaptation to evolutionary needs (2). In avian skin development, the emergence of multiple cell condensations leads to the periodic arrangements of feather germs. Localized growth zones increase cell numbers producing organ elongation in a directed fashion to begin to shape avian beaks (3) and skin appendages (4). During feather branch formation, alternating localized differentiated/apoptotic modules in feather filament epithelia become barbs and interbarb space (5), further configuring the final feather shape. The boundary and durations of these different activity modules can work in coordination to build and sculpt complex architectures during organ development and regeneration.

These activity modules are likely to be initiated by morphogen gradients emitted from organizers that specify axial polarity, first in the body axis and later in organ primordia (6). Remarkable examples of morphogen gradients regulating activity modules have been identified in the specification of the anterior–posterior (A–P) axis by a decapentaplegic gradient in the *Drosophila* wing (7) and a sonic hedgehog gradient in the limb bud zone of polarizing activity (8). How an early chemical morphogenetic signal is converted to multicellular mechanical processes and how its performance can be adjusted was studied in a chicken feather model. Feather primordia on embryonic chicken dorsal skin autonomously elongate with a common orientation along the original body A–P axis in vivo and in cultured skin explants. These observations suggest the feather elongation process is both precise and robust. In chickens, individual feathers appear on the dorsal skin as a local epithelial thickening around Stage 29 (St. 29) (9). Soon afterward the underlying dermis condenses to form a round, radially symmetric feather primordium. This early stage feather bud first grows radially during the symmetric short bud stage. The bud apex then shifts posteriorly during the asymmetric short bud stage. The feather bud continues to elongate and its height exceeds its diameter (long bud stage). At this point the bud tilts caudally. After the long bud stage the feather invaginates and develops its follicle structure (follicle stage). Through this series of morphological changes A–P and then proximal–distal (P–D) axes emerge in the feather buds.

Previous efforts to unveil the molecular mechanism of feather polarity revealed dynamic molecular expression patterns from the short symmetric bud stage to the follicle stage. In general, these expression patterns show three domains within the bud: anterior, central, and posterior. Bone morphogenetic protein 2 (*BMP2*) is in the anterior epithelium and *Bmp4* is in the anterior mesenchyme (10). *Notch1* is in the central mesenchyme and (11) Delta-like 1 (*Dll1*) is in the posterior mesenchyme (11, 12). Wingless-int (*Wnt*)*7a* is in the posterior epithelium (13). However, two critical questions

Significance

How are specific organs shaped? To convert organ primordia from small domes to polarized, thin, conical structures, the orientation and duration of the elongation process must be carefully regulated. Using a feather bud elongation model, we identify a molecular module that directs precisely oriented elongation by converting a chemical gradient into a sharp boundary zone, which mediates mechanical processes. The module involves wingless-int (Wnt)7a, β-catenin, and nonmuscle myosin IIB and is modulated by Notch activity. Our mathematical simulations confirm the module's effect on reducing variations and fluctuations in the system via gradient-threshold conversion.

Author contributions: A.L. and C.-M.C. designed research; A.L., M.C., T.-X.J., and P.W. performed research; M.C., T.-X.J., P.W., and Q.N. contributed new reagents/analytic tools; A.L., M.C., Q.N., R.W., and C.-M.C. analyzed data; and A.L., M.C., Q.N., R.W., and C.-M.C. wrote the paper.

The authors declare no conflict of interest.

This article is a PNAS Direct Submission.

[1]To whom correspondence should be addressed. E-mail: cmchuong@usc.edu.

This article contains supporting information online at www.pnas.org/lookup/suppl/doi:10.1073/pnas.1219813110/-/DCSupplemental.

remain to be answered. How do these pathways cross-talk with one another? How does this cross-talk network regulate cell behavior to produce oriented bud elongation? Our current study sheds light on these issues.

Results

Transplantation Experiments Reveal Localized Polarizing Activity Within the Posterior Feather Bud. To investigate where feather bud polarizing activity resides during bud growth, we exchanged different parts of late symmetric short bud stage feather buds on chicken embryonic skin explants. The donor dermis was 1,1′-dioctadecyl-3,3,3′3′-tetramethylindocarbocyanine perchlorate (DiI) labeled. Anterior-to-anterior (n = 4) or posterior-to-posterior (n = 5) transplantation did not alter feather bud elongation (Fig. 1 *A* and *B*). Replacing a posterior bud region with an anterior bud abolished bud growth (Fig. 1*C*; 48 h; n = 8). In contrast, replacing the anterior region with a posterior region caused the chimeric bud to grow two tips 180° apart after 48 h (Fig. 1*D*; 48 h; n = 14). Replacing the left lateral half of a feather bud with a DiI-labeled posterior bud caused the chimeric bud to develop two tips oriented about 90° apart (Fig. 1*E*; n = 12). In these dual-tipped feather buds, tip orientations are consistent with those of the original and transplanted posterior buds.

Identifying Cellular and Molecular Activities Present in the Polarizing Zone During the Time of Oriented Bud Elongation. Previously we found that the earliest feather polarity cues come from the epithelium during development (11). Endogenous *Wnt7a* was expressed in the posterior bud epithelium during the symmetric short bud stage. Ectopic expression of Wnt7a caused "posteriorization" of both feather bud morphology and molecular expression (13). Our past and present findings suggest that the *Wnt7a* expressing posterior epithelium is the potential signaling center directing feather bud growth. Nuclear β-catenin positive cells were also observed during normal feather bud development (14). We examined the subcellular localization of β-catenin in feather buds from the symmetric short bud stage to the early follicle stage (Fig. S1 *A*–*D*). Nuclear β-catenin positive cells are observed in posterior bud dermis beginning in the symmetric short bud stage. Their number increases throughout the asymmetric short bud and early long bud stage and decreases rapidly thereafter (Fig. 2*B*). Confocal microscopy at the asymmetric short bud stage and early long bud stage showed the dermal nuclear β-catenin zone (DBZ) is crescent shaped with relatively homogeneous intensity. On the edge of this crescent the intensity of nuclear β-catenin drops precipitously (sharp boundary) (Fig. 2*A*). Interestingly, in the transplantation experiments described above, buds without DBZs did not elongate (Fig. 1*C*; 14 h). Buds with two DBZs developed two separate distal ends (Fig. 1 *D* and *E*; 14 h). These observations imply a correlation between the DBZ and feather polarizing activity.

Nuclear β-catenin positive cells were also observed in anterior bud epithelium before the long bud stage (Fig. 2*C* and Fig. S1 *A* and *B*; arrowheads). However, three observations suggest this epithelial nuclear β-catenin zone may not contain polarizing activity. First, in skin explants epithelial nuclear β-catenin diminishes to undetectable levels at the symmetric short bud stage whereas the buds can still elongate. Second, growth can be disrupted whereas the epithelial nuclear β-catenin zone remained intact (e.g., culturing skin in media containing 5 μM DAPT, a γ-secretase inhibitor). Finally, the epithelial nuclear β-catenin zone diminishes in area from the symmetric short bud stage (14) and completely disappears by the long bud stage. The temporal and spatial dynamics of this zone (Fig. 2*G*) suggest that it is likely involved in morphogenetic events occurring before bud elongation.

Asymmetry in organ morphology may be caused by several possible mechanisms. Previous work has suggested that localized cell proliferation can contribute to the A–P axis of the feather buds (4, 15). Hence, we examined whether there are any spatial correlations between the DBZ and proliferating dermal cells. BrdU pulse labeling revealed that dermal cell proliferation is homogeneous at the symmetric short bud stage and becomes localized to the posterior bud at the asymmetric short bud stage. However, the range of this proliferation zone is much larger than that of the DBZ and shifts distally thereafter (Figs. S1 *A′*–*D′* and S2 *A* and *B*). The DBZ starts to appear in the posterior bud at symmetric short bud stage and generally maintains its position

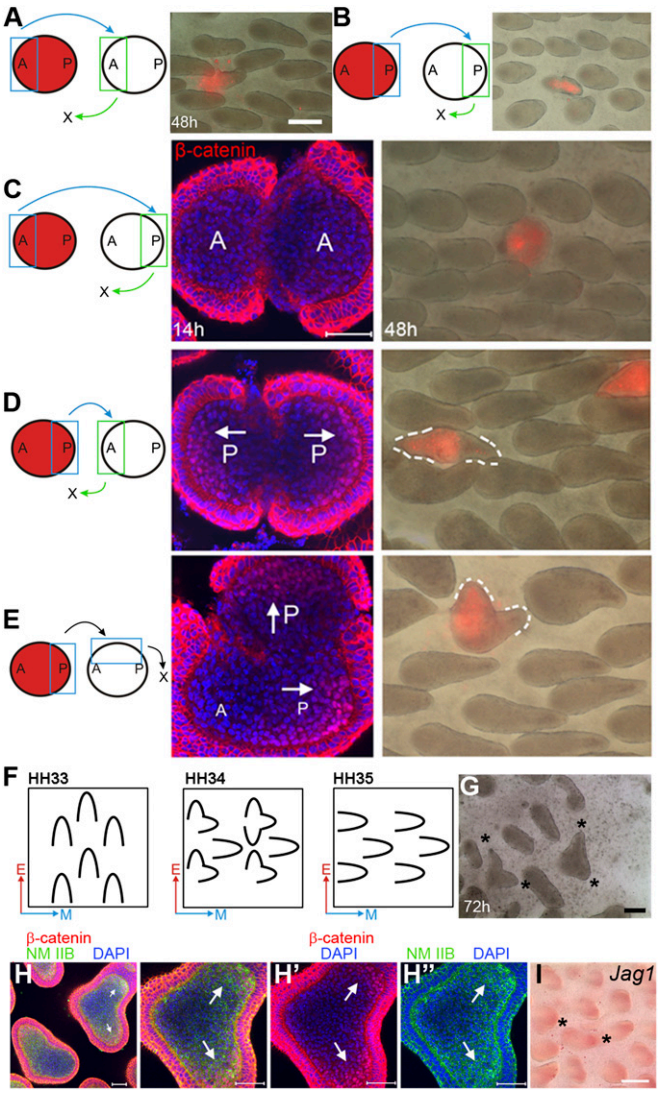

Fig. 1. Exchanging different parts of feather buds indicates that the nuclear β-catenin positive dermis bears polarizing activity. This result is supported by epithelial–mesenchymal recombination and rotation experiments (EMRR). (*A*–*E*) Exchanging different parts of feather buds. Chimeric bud morphology observed 48 h after surgery. Blue: transplant donor site. Green: transplant recipient site. (Red) DiI-labeled donor tissue. (Scale bar: 250 μm.) (*A*) Anterior-to-anterior transplantation. (*B*) Posterior-to-posterior transplantation. (*C*) Replacing posterior bud with anterior bud. (*D*) Replacing anterior bud with posterior bud. (*E*) Replacing left lateral bud with posterior bud. (*C*–*E*) Confocal images of the corresponding chimeric buds stained for β-catenin 14 h after surgery. (*F*) Summary of EMRR experiments. A–P axis orientation for epithelium (red arrows) and dermis (blue arrows). (*G*) St. 34 chicken embryo dorsal skin cultured for 72 h after EMRR shows bifurcated orientation (*). (Scale bar: 1 mm.) (*H*) Same stage specimen cultured 20 h after EMRR. Arrows: nuclear β-catenin positive dermis and up-regulated nonmuscle myosin (NM) IIB. (*H′*) and (*H″*) show the β-catenin and NM IIB pattern, respectively. (Scale bar: 50 μm.) (*I*) *Jag1* expression increases at the location of nuclear β-catenin positive dermis (*). (Scale bar: 500 μm.)

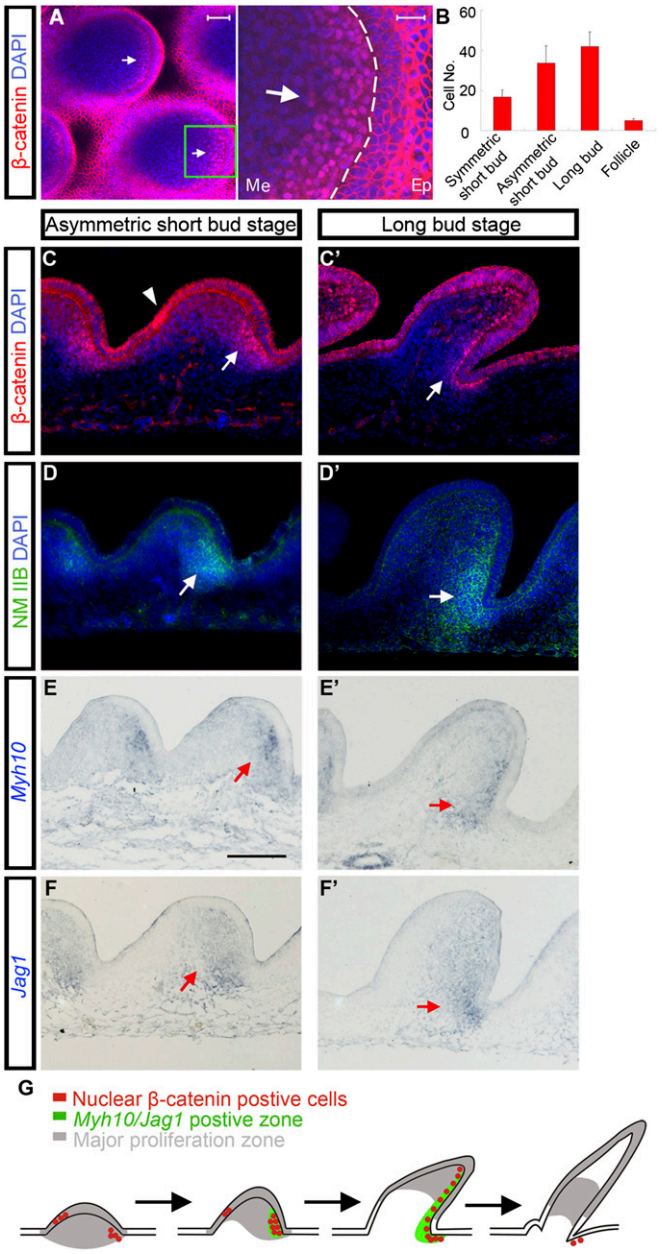

Fig. 2. A zone of nuclear β-catenin positive cells is localized to posterior dermis during feather bud elongation. This zone has high levels of NM IIB and *Jag1*. (*A*) Confocal pictures of E8 chicken embryo dorsal skin feather buds at the asymmetric short bud stage show nuclear β-catenin positive dermis. Green boxes show the magnified region. Ep, epithelium; Me, mesenchyme. (Scale bar: 50 μm and 20 μm, respectively.) (*B*) Counts of dermal cells with nuclear accumulated β-catenin from sagittal sections of feather buds at the symmetric short bud stage, asymmetric short bud stage, long bud stage, and follicle stage. For each stage $n = 12$. (*C*) and (*C′*) β-catenin staining on sagittal sections of feather buds at asymmetric short bud and long bud stage, respectively. (Arrows) Nuclear β-catenin positive dermis. (Arrowheads) Nuclear β-catenin positive epithelium. (Scale bar: 50 μm.) (*D–F′*) High-level NM IIB and *Jag1* are detected in the nuclear β-catenin positive dermis. *Myh10* encodes NM IIB heavy chain. (Scale bar: 100 μm.) (*G*) Schematic summary of the results.

close to the posterior epithelial–mesenchymal boundary thereafter (Figs. S1 *A–D* and S2 *A* and *B*). Confocal images of feather buds stained with proliferating cell nuclear antigen (PCNA) and β-catenin show no significant overlap between the two (Fig. S2*C*). Due to the different spatial distributions of proliferating cells and nuclear β-catenin positive cells, it is unlikely that nuclear β-catenin in the DBZ directly controls cell proliferation. We also tried to examine the distribution of apoptotic cells using the terminal deoxynucleotidyl transferase dUTP nick end labeling (TUNEL) assay. No areas in feather bud dermis were enriched for apoptotic cells (Fig. S2*D*). Therefore, although cell proliferation may play a role, other mechanism(s) may also provide significant contributions to the polarized elongation process.

Besides β-catenin, we also found that the DBZ is enriched for *Jag1* (Notch ligand) and nonmuscle myosin (NM) IIB (*Myh10*) mRNAs during the asymmetric short bud and long bud stages (Fig. 2 *D–F′*). Next, we investigated the relationship between these molecules in feather bud elongation through functional perturbation experiments.

Perturbation of the Dermal Nuclear β-Catenin Positive Zone Causes Random Orientation of Feather Buds. To evaluate the relationship of the DBZ and feather polarizing activity, we first performed epithelial–mesenchymal recombination and rotation experiments (EMRR) (11) (Fig. 1 *F* and *G*). EMRR of St. 34 chicken dorsal skin yield numerous dual-tip feather buds. The two tips follow the epithelial and mesenchymal A–P orientations, respectively. β-catenin staining 20 h after EMRR showed the presence of two DBZs. Their locations were consistent with the positions of the two tips (Fig. 1 *H* and *H′*). This result confirms the close relationship between the DBZs and polarizing activity.

To evaluate the functional role of the DBZ in feather bud morphogenesis, we used electroporation to introduce Replication Competent Avian Sarcoma Virus (RCAS)-β-catenin proviral plasmids to the left side of E3 chicken embryos (see experimental details in *Methods*). This proviral plasmid can generate active virus misexpressing a constitutively active form of β-catenin in cells. The right side serves as an internal control (Fig. 3*C*). Most RCAS-β-catenin–treated embryos demonstrated significant feather misorientation on the treated side 6 d after treatment (62/72) (Fig. 3 *B*, *B′*, and *D*). The severity of bud fusion in the remaining samples prevented us from assessing feather orientation. Fusion, an abnormality in determining the bud-vs.-interbud area, occurs before polarization and may be related to the presence of nuclear β-catenin in the epithelium. RCAS-GFP–treated control embryos show that the viral vector has no effect on feather orientation or bud fusion (31/35) (Fig. 3 *A* and *A′*).

To better understand the topological relationship between the DBZ and directional feather growth, we analyzed the distribution of nuclear β-catenin positive cells in the misoriented buds by confocal microscopy (Fig. 3*E*). These buds retained their endogenous DBZ (distal; green arrows) but have acquired an ectopic DBZ located within the lateral regions of the bud, oriented 90° from the original DBZ (proximal; red arrows). The location of the bud tip was consistent with the location of the ectopic DBZ. The buds also retained a small, visible bulge that colocalizes with the endogenous DBZ. In 3D reconstruction we can see the endogenous and exogenous DBZs (Fig. 3*E′*).

We also blocked canonical Wnt signaling in E7 chicken skin explants using endo-IWR1 (an axin stabilizer) or dickkopf 1 (DKK1) overexpression (16). In both cases feather bud elongation was inhibited and feather bud polarity became obscured (Fig. S3*A*). These results demonstrate that the DBZ is necessary and sufficient to mediate the polarized elongation of feather buds.

Dermal Nuclear β-Catenin Activates Nonmuscle Myosin IIB Expression to Mediate Polarized Cell Rearrangement. Polarized tissue morphogenesis can be attributed either to polarized cell rearrangement (17), oriented cell division (18), or localized cell proliferation/apoptosis (5, 19). Previously we tried to examine the orientation of mitosis through γ-tubulin staining. We did not observe a clear alignment of cell division orientation. To test whether polarized cell rearrangement contributes to feather bud elongation we examined the expression patterns of NM II isoforms. These

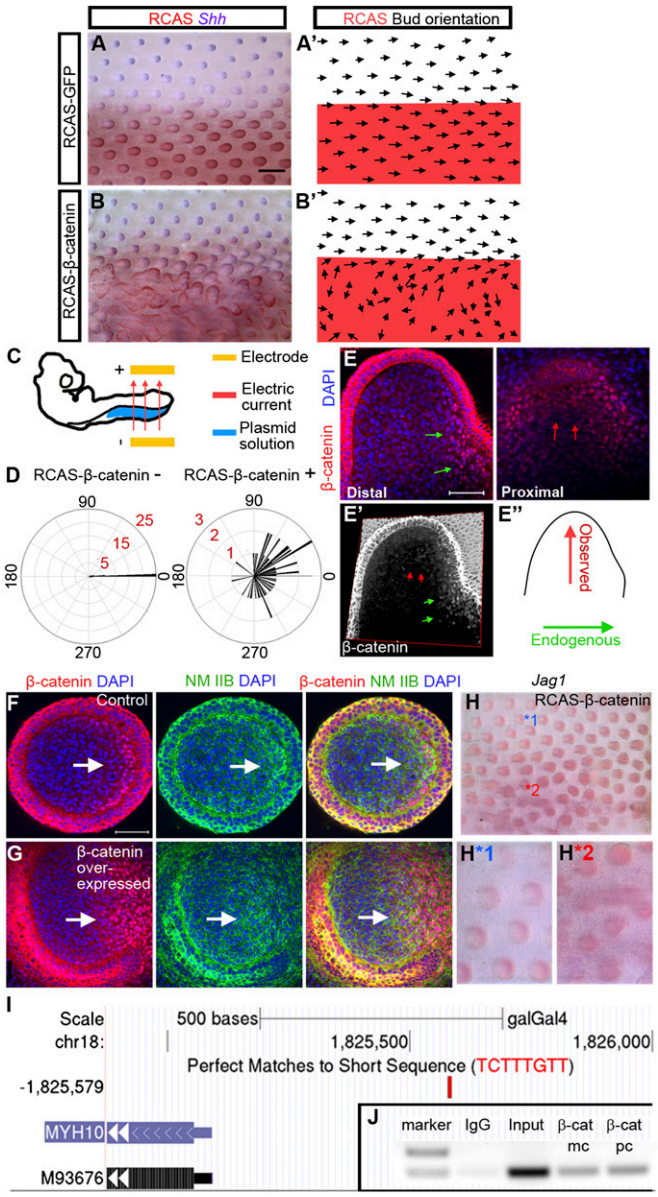

Fig. 3. Misexpression of stabilized β-catenin caused drastic feather misorientation and up-regulation of NM IIB and *Jag1*. (*A*) E9 chicken embryo with RCAS-GFP electroporated to its left side at E3. (blue, *Shh* in situ; red, RCAS staining) (n = 35). (B) E9 chicken embryo with RCAS-β-catenin electroporated to its left side at E3 (n = 72). (Scale bar: 500 μm.) (*A′*–*B′*) Schematic drawing of feather orientation and RCAS positive area. (*C*) E3 embryo electroporation setup. (*D*) Summary of feather bud orientation relative to the body A–P axis in RCAS-β-catenin negative (n = 45) and positive (n = 57) areas, respectively. (*E*) Confocal images at two different levels (proximal and distal) of a misoriented, β-catenin overexpressing feather bud. The distal view shows a nuclear β-catenin zone at the original posterior region (green arrows). The proximal view shows a second nuclear β-catenin zone in the new, reoriented posterior region (red arrows). (*E′*) 3D reconstruction of β-catenin staining pattern in *E*. (*E″*) Schematic representation of the original and new bud A–P axis. (*F* and *G*) Control and β-catenin overexpressed short feather buds stained with β-catenin, and NM IIB. (Scale bar: 50 μm.) (*H*) *Jag1* whole mount in situ of RCAS β-catenin expressing skin. Enlargement of feather buds from a control (*H**1) and RCAS β-catenin expressing (*H**2) region in *H*. (*I*) Potential WRE located upstream of *Myh10* (shown in University of California, Santa Cruz genome browser. M93676 is *Myh10* accession code in GenBank). (*J*) ChIP-PCR result. β-cat mc, monoclonal β-catenin antibody; β-cat pc, polyclonal β-catenin antibody.

proteins are highly conserved motor proteins for cell motility (17, 20). Mammals have three NM II isoforms (A, B, and C), distinguished by the nonhelical tail region of the heavy chains (21). These mammalian heavy chain isoforms are encoded by *Myh9* (NM IIA), *Myh10* (NM IIB), and *Myh14* (NM IIC). *Myh14* is not found in the chicken genome. Chicken *Myh9* expression is restricted to the vasculature (Fig. S4 *C* and *C′*). Chicken *Myh10* RNA and protein are both present at high levels in the DBZ during the asymmetric short bud and long bud stages (Fig. 2 *D*, *E*, and *E′* and Fig. S4 *D* and *D′*).

NM IIB expression dynamics suggests it may be a target of β-catenin signaling. We located a perfect match to the Wnt-response element (WRE; C/T-C-T-T-T-G-A/T-A/T) at −494 to −487 upstream of the *Myh10* transcription start site (Fig. 3*I*). WRE is a conserved binding site for Lef/Tcf proteins (22). To confirm binding of β-catenin to this potential WRE we did ChIP analysis on chromatin isolated from E8 chicken dorsal skin using anti-β-catenin antibodies. The chromatin was amplified by PCR with primers across this potential WRE. Both monoclonal and polyclonal β-catenin antibodies can successfully pull it down (Fig. 3*J*).

Previous studies showed that NM IIB works through the actin network (21). The actin network is randomly arranged before NM IIB up-regulation but becomes aligned along the posterior epithelium–mesenchyme boundary after NM IIB up-regulation (Fig. S4 *A*, *B*, and *B′*). This observation indicates that NM IIB is functionally active in feather buds. We next compared the NM IIB expression pattern in β-catenin overexpressing and normal feather buds. The area expressing NM IIB expanded in β-catenin overexpressing dermis (Fig. 3*G*) compared with the control (Fig. 3*F*). In St. 34 EMRR experiments, the two DBZs in the "dual-tip" buds both have high levels of NM IIB (Fig. 1 *H*, *H1*, and *H2*). In contrast, NM IIB expression decreases when the DBZ disappears upon DAPT (10 μM) and endo-IWR1 (10 μM) treatment (Fig. S3 *C* and *D*). Additionally, we treated the E7 skin explants overexpressing stabilized β-catenin with 10 μM Blebbistatin, a selective inhibitor for myosin II. Misoriented feather bud elongation caused by ectopic β-catenin was inhibited (Fig. S3*E*). Together, these data demonstrate that NM IIB works downstream of β-catenin signaling.

To test whether NM IIB is involved in cell rearrangement during feather bud elongation, we blocked its function with Blebbistatin. In cell culture, E7 chicken dorsal skin fibroblasts were treated with DMSO or 10 μM Blebbistatin. Cell behavior was documented for 12 h after treatment. Most control group cells showed bipolar, elongated cell shapes (Fig. 4*A*, *Left*) and moved along their long axis (Fig. 4*A′*, *Left*), whereas almost all Blebbistatin-treated cells showed multipolar shapes (Fig. 4*A*, *Right*). Their trajectories were random compared with controls (Fig. 4*A′*). Many Blebbistatin-treated cells made sudden and significant turns during migration, which occurred rarely in control cells (Fig. 4*D*). These results confirm the previous report that blocking NM IIB function affects cell rearrangement patterns (23).

In tissue culture, E7 chicken skin explants were treated with different doses of Blebbistatin. Blebbistatin treatment inhibited feather bud elongation in a dose-dependent manner. Feather bud polarity was lost at 50 μM (Fig. 4 *B* and *E*). Rho-kinases (ROCK) are known be involved in NM activation (24). Treating specimens with Y27632 (ROCK inhibitor) also generated a similar inhibitory phenotype (Fig. 4*C*). To further examine the role of altered cell rearrangement patterns on feather bud morphology, some posterior cells of late symmetric short bud stage skin explants treated with 10 μM Blebbistatin or DMSO were labeled (Vybrant cell tracer, Invitrogen). Time-course images (Fig. 4 *F* and *G*) show that in control explants these cells gradually aligned parallel to the axis of elongation, whereas cells in Blebbistatin-treated specimens scattered randomly from their site of origin. Labeled dermis cells in the anterior bud did not move much in either DMSO or Blebbistatin-treated specimens (Fig. 4 *H* and *I*). The directional rearrangement of posterior dermal cells is consistent with changes in the DBZ configuration: the DBZ decreases from ~3–5 cell

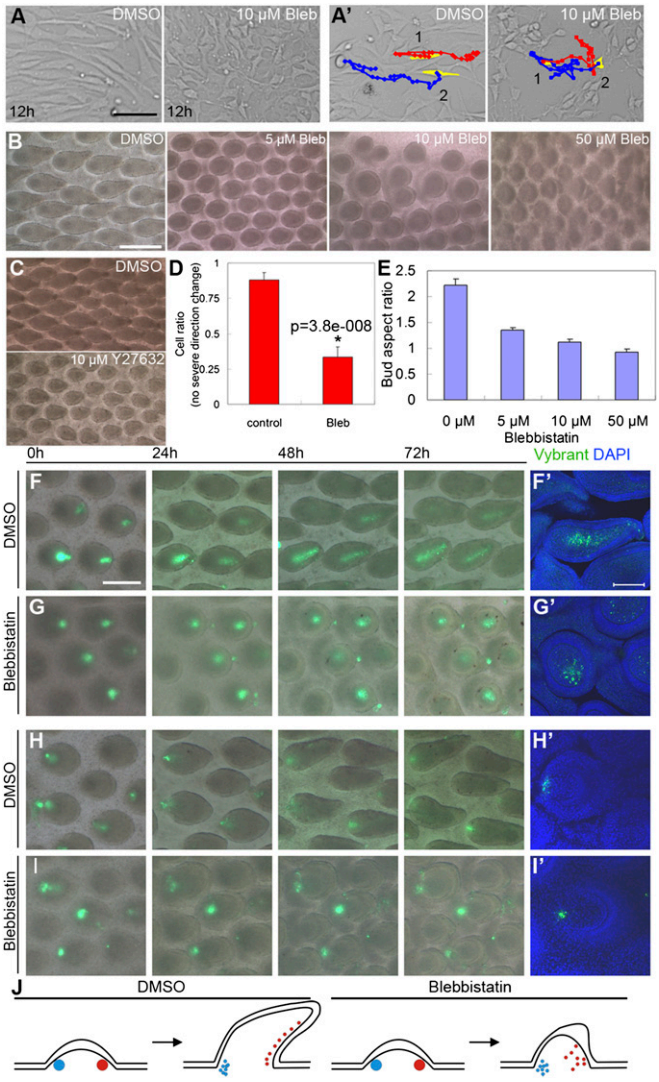

Fig. 4. Blocking NM IIB function disrupted fibroblast migration patterns in vitro and inhibited feather bud elongation in vivo. (*A*) E7 chicken embryo dorsal skin fibroblasts transfected with RCAS-*β*-catenin to mimic posterior dermis were cultured 12 h in media containing DMSO or 10 μM Blebbistatin (Bleb), respectively. Notice the difference in cell shape. (*A′*) Most control cells moved in the direction of their long axis, whereas many Blebbistatin treated cells moved randomly. (Scale bar: 100 μm.) Red, blue lines show the movement trajectory of two cells artificially colored yellow at time 0. (*B*) Skin explants cultured 4 d with DMSO (control) and different doses of Blebbistatin, respectively. (Scale bar: 500 μm.) (*C*) Inhibition of bud elongation by Blebbistatin could be phenocopied by treatment with Y27632 (ROCK inhibitor). (*D*) Statistics of cell rearrangements for *A′*. For details please see *Statistics*. (*E*) Feather bud aspect ratio (length/width) at different Blebbistatin concentrations (n = 20 for each treatment condition). (*F–I*) Time-course pictures of Vybrant dye labeled posterior (*F* and *G*) and anterior (*H* and *I*) bud dermis in control and Blebbistatin-treated buds. (Scale bar: 250 μm.) (*F′–I′*) Confocal images of feather buds from the corresponding 72-h explants. (Scale bar: 100 μm.) (*J*) Schematic representing cell tracking results for the anterior (blue) and posterior (red) dermis.

layers at the asymmetric short bud stage to ∼1–2 layers at the long bud stage (Fig. S1 *B* and *C*). Collectively, these results demonstrate that the DBZ induces NM IIB to mediate polarized cell rearrangements during feather bud elongation (Fig. 4*J*).

We further investigated the cell rearrangement pattern through dual dye tracking experiments. Two separate populations of mesenchymal cells were labeled on the right (Invitrogen Qtracker) and left (Vybrant Cell Tracker) lateral side of the bud. Through time-lapse imaging we found that cells from these two populations can mix together to form a broad line, suggesting the bud mesenchymal cells could rearrange perpendicular to the direction of bud elongation (Fig. S5). Therefore, we hypothesize that NM IIB may mediate cell intercalation in feather bud elongation, as has been reported in other systems (20). This hypothesis will be tested further in the near future with higher resolution live tissue imaging.

Notch Signaling Is Activated by the Nuclear *β*-Catenin Positive Dermis and Sustains the DBZ Through a Positive Feedback Loop. Molecules along the Notch pathway showed polarized expression patterns in feather buds (11). *Jag1*, a Notch ligand, is expressed in the DBZ (Fig. 2*G*) during the symmetric short bud and long bud stages. *Jag1* was up-regulated upon *β*-catenin overexpression (Fig. 3*H*). In addition, *Jag1* is expressed in both DBZs produced by the EMRR experiment (Fig. 1*I*). Blocking β-catenin signaling with endo-IWR1 also significantly decreased the expression of *Jag1* (Fig. S3*B*). These findings indicate that *Jag1* expression is induced by *β*-catenin signaling.

To further understand Notch pathway function in feather bud elongation, we used DAPT to block Notch signal transduction. Feather orientation was significantly randomized even at very low drug concentrations (5 μM), and feather bud elongation was inhibited at higher DAPT doses (Fig. 5 *A–C*). These phenotypes imply that the Notch pathway may be activated by *β*-catenin signaling to mediate polarized feather bud elongation. To confirm that the phenotype of DAPT-treated samples was due to Notch inhibition, we treated the DAPT specimens with RCAS-NICD (Notch intracellular domain, the constitutively active form of *Notch1*). Misorientation by DAPT-treated feather buds generally does not happen in the RCAS-NICD positive area (Fig. 5 *D*, *E*, and *E′*; 4/8), but RCAS-NICD can produce other phenotypes making rescue difficult to discern in the remaining four samples.

However, RCAS-NICD alone did not induce altered feather orientation (Fig. S6). Therefore, we compared the expression pattern of Notch pathway members, *β*-catenin, and NM IIB between feather buds from DMSO- and DAPT-treated explants. *Notch1* expression was lost in the bud dermis but appeared in an abnormal epithelial invagination in DAPT-treated specimens (Fig. 5 *H* and *H′*). *Hey1*, a classical Notch target gene, also disappeared in the bud dermis but became expressed in the interbud epithelium (Fig. 5 *I* and *I′*). *Jag1* expression was undetectable in DAPT specimens, even at low concentrations (5 μM; Fig. 5 *J* and *J′*). DAPT treatment also causes decreased *Jag1* expression in other systems (25, 26). Nuclear *β*-catenin was nearly completely lost in 10 μM DAPT-treated specimens and NM IIB levels were very low throughout the bud dermis compared with controls (Fig. 5 *F* and *G*). Even a low DAPT dose (5 μM) significantly decreased the DBZ area and altered its configuration (Fig. 6 *D* and *D′*). These observations imply that Notch signaling helps to stabilize the DBZ spatial configuration.

Notch Signaling Converts the Highly Variable Wnt Gradient into a Spatially Well-Defined, Localized Nuclear *β*-Catenin Dermal Response. Wnt7a was expressed in the posterior bud epithelium during the short bud stage, so the spatial and temporal concurrence of DBZ emergence with Wnt7a expression suggests a potential connection between the two (Fig. 6*A*). We examined this potential connection by comparing the effects of placing Wnt7a (0.2 M) or control (BSA) soaked beads on E7 chicken dorsal skin dermis. After 24 h significant *β*-catenin accumulation was observed in the Wnt7a group but not in the control group, indicating Wnt7a is an upstream trigger of nuclear *β*-catenin (Fig. 6 *C* and *C′*). This relationship has also been revealed in other systems (27, 28).

However, the spatial distributions of Wnt7a and nuclear *β*-catenin intensity exhibit two major differences. By immunostaining we found Wnt7a protein showed a punctate expression pattern in the bud dermis. The density is highest at the posterior dermal–epidermal boundary (source) and decreases toward the anterior

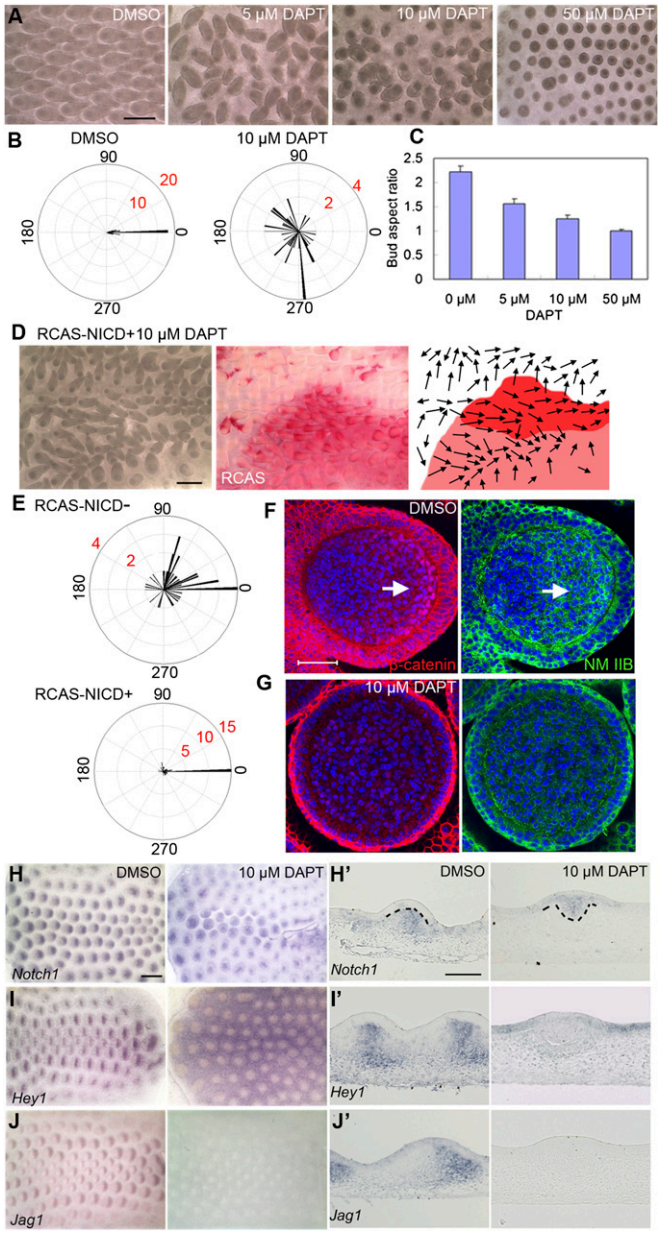

Fig. 5. Inhibition of Notch signaling by DAPT causes drastic feather misorientation and dose-dependent inhibition of bud elongation. Meanwhile DBZ nuclear β-catenin and NM IIB level are dramatically decreased. (*A*) E7 skin explants cultured for 4 d with DMSO or different doses of DAPT. (*B*) Summary of feather bud orientation relative to the body A–P axis upon DMSO ($n = 40$) or 10 μM DAPT ($n = 40$) treatment, respectively. (*C*) Feather buds' aspect ratio at different DAPT concentrations ($n = 20$ for each concentration). (*D*) E8 chicken embryo dorsal skin (electroporated with RCAS-NICD at E3) cultured with 10 μM DAPT for 72 h. Red signal shows RCAS positive area. Arrows in the schematic drawing represent feather bud orientation. (*E*) Divergence of feather bud orientations from the body A–P axis in the RCAS-NICD negative and positive area, respectively ($n = 44$ for each condition). (*F* and *G*) Confocal image of a feather bud on E7 skin explant cultured for 1.5 d with DMSO and DAPT (10 μM) in media, respectively. (Arrow) nuclear β-catenin positive cells. (Scale bar: 50 μm.) (*H–J*) Whole-mount in situ hybridization of DMSO- and DAPT-treated skin explants (after 40 h in culture) with *Notch1, Hey1, Jag1* probes, respectively. (Scale bar: 500 μm.) (*H′–J′*) Section in situ hybridization of DMSO- and DAPT-treated skin explants with the three probes, respectively. (Scale bar: 100 μm.)

regions of the bud, forming a molecular gradient (Fig. 6 *B*, *D*, and *D′*). Similar to some other reported organizer morphogens, this gradient shows an exponential decay, fitting Wolpert's diffusion degradation model (29). However, due to its punctate nature, measurements of this gradient fluctuate (in contrast with the smooth curve of a deterministic gradient). Meanwhile, the slope of the gradient exhibits relatively large variations among individual buds (Fig. 6*E*). Hence, this process is "noisy" from the mathematical perspective. In contrast, the intensity of the nuclear β-catenin decreases precipitously ~20 μm from the posterior epithelial–mesenchymal boarder, forming a sharp DBZ boundary, and this distance is quite consistent between different buds (Fig. 6 *D*, *D′*, and *E*).

How is the noisy Wnt7a gradient converted to a sharp on/off downstream response? We speculate that Notch signaling may be involved in this process. Indeed, inhibiting Notch signaling (5 μM DAPT) induces the nuclear β-catenin plateau to fragment into multiple small clusters (composed of ~1–6 cells) randomly distributed along the epithelial–mesenchymal boundary (Fig. 6 *D*, *D′*, and *E*). This implies that the response to Wnt signaling became noisy after Notch signaling was blocked.

Based on these observations and evidence from others (30, 31), we built a Wnt–Notch cross-talk model to investigate the sharp on/off response (Fig. 6*F*, black arrows). In the model, Wnt7a increases nuclear β-catenin, which induces *Jag1* expression. *Jag1* and Notch mutually inhibit each other's expression within the same cell but their interactions between neighboring cells activate Notch signaling. Notch signaling would positively feedback to enhance localization of β-catenin to the nucleus.

To test the proposed network, we performed 1D and 2D simulations (Table S1) and examined whether this model can achieve the observed conversion from Wnt to nuclear β-catenin (Fig. 6 *G* and *H*). First, without including Wnt–Notch cross-talk, we found the noisy Wnt7a gradient is converted into multiple small nuclear β-catenin clusters (Fig. 6*H*), consistent with our experimental observation on DAPT-treated specimens. However, when Wnt–Notch cross-talk was added, we found isolated clusters of nuclear β-catenin (Fig. 6 *G* and *H*). In this case, there is an expansion of the *Jag1* positive area with Notch expression in the rest of the domain due to lateral inhibition, as observed in normal feather buds. As a result, Notch signaling appears at the *Jag1* and *Notch1* expression interface, leading to a sharp boundary which reduces fluctuations in nuclear β-catenin activity, thus forming a more uniform DBZ. These simulations show an interesting dual role of the Wnt–Notch cross-talk module: It converts a graded gradient into a sharper on/off response as well as reduces cell-to-cell variability in response to the signal.

Discussion

Here, we identified a unique local molecular module that can generate oriented organ elongation, which then contributes to organ polarity. The molecular module uses an epithelial signaling component and a dermal polarizing zone characterized by the presence of a local nuclear β-catenin centered molecular module. The execution of morphogenetic activity is mediated by NM IIB. Upstream regulation comes from epidermal Wnt signaling (the core pathway). Its activity and boundary is maintained and modulated by Notch signaling (the modulatory pathway). This molecular network is summarized in Fig. 7.

A crucial point in organogenesis is how the organ primordia set up signaling organizers and how these signals shape and orient organs. In the limb bud, retinoic acid and Shh were shown to possess polarizing activity (6). Using a similar tissue transplantation strategy, we identified the zone with feather polarizing activity, which is positioned in the posterior short feather buds. However, when we characterized the molecular properties of this zone, we found that its activity is not based on Shh. Rather, it is based on a Wnt/β-catenin /NM IIB module which shows cross-talk with Notch signaling. The Wnt pathway has been implicated in setting organ polarity during multiple morphogenetic processes. Canonical Wnt signaling helps establish the primary body

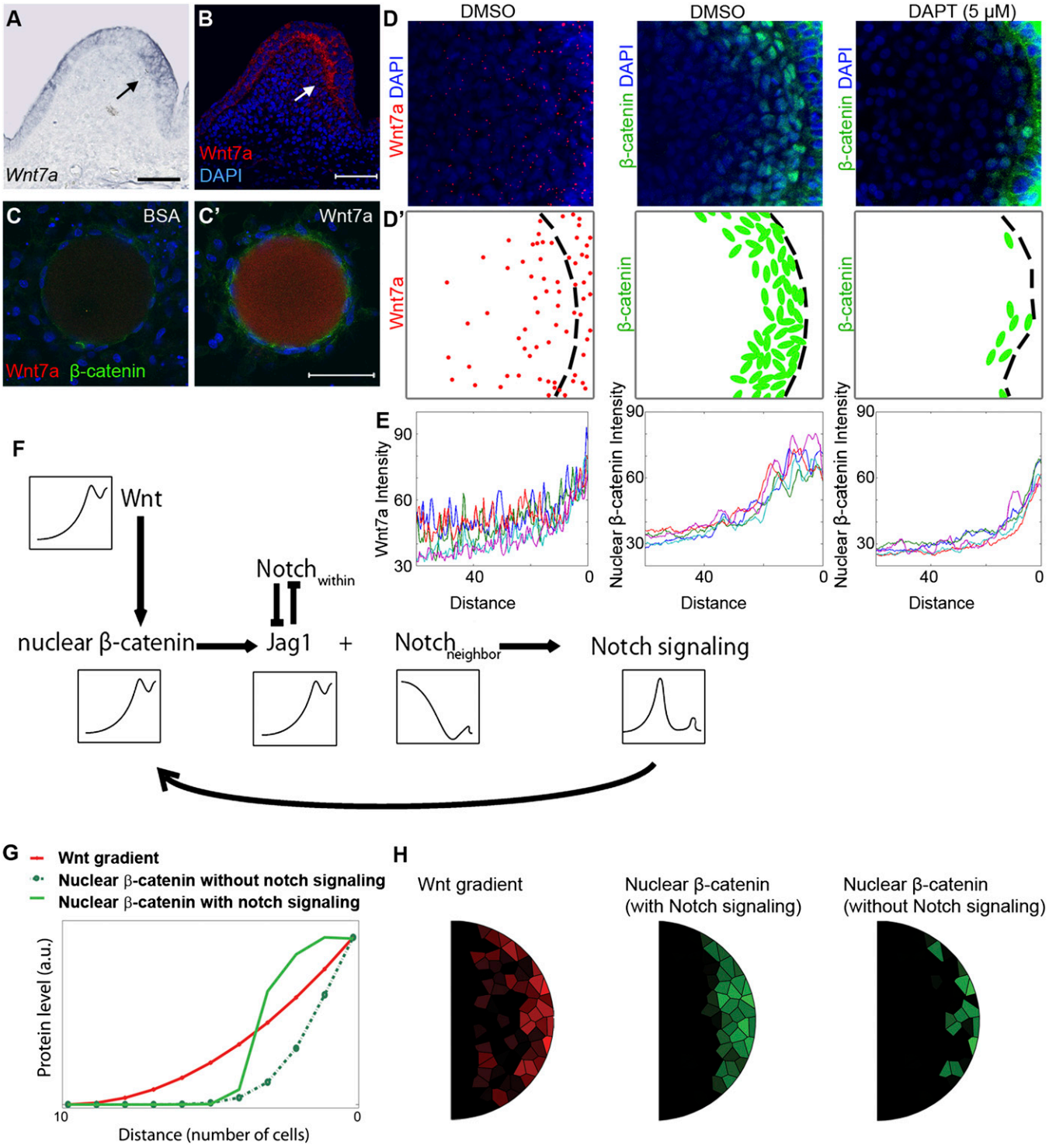

Fig. 6. Mathematical modeling of Wnt–Notch cross-talk simulates the change from a noisy, gradual Wnt gradient to a definitive threshold Wnt response. (*A*) Section in situ hybridization for *Wnt7a* (arrow) in feather buds. (*B*) Fluorescent staining of Wnt7a. (*C* and *C′*) Effect of BSA and Wnt7a (0.2 M) soaked beads on E7 chicken skin dermis cultured for 24 h. (Scale bar: 50 μm.) (*D*) Wnt7a and β-catenin staining in control and 5 μM DAPT-treated feather buds (compact confocal Z-stack pictures). (*D′*) Schematic summary of *D*. (*E*) Wnt7a, β-catenin signal intensity measured from five feather buds for each condition (distance is calculated from the posterior epithelial–dermal boundary to the center of the bud). (*F*) Wnt–Notch cross-talk relationships used for mathematical modeling. (*G*) Simulation (1D) shows Wnt–Notch cross-talk can help nuclear β-catenin form an ultrasensitive response to Wnt ligand. (*H*) Simulation (2D) results.

axis in a number of species, as well as to specify neural plate A–P axis in *Xenopus laevis* (32). However, most reports infer the noncanonical Wnt/planar cell polarity pathway (PCP) as a key polarizing organizer (33).

Common cellular mechanisms for the organ polarization process include alignment of cell division orientation, localization of cell proliferation/apoptosis, and polarized cell rearrangement (including directional cell migration, intercalation).

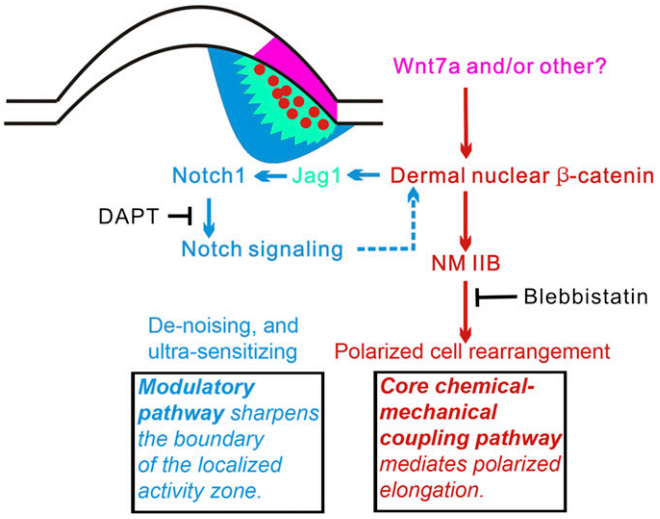

Fig. 7. Summary of the core and modulatory molecular modules for polarized elongation during feather bud morphogenesis. Purple, Wnt7a and/or other Wnt molecules from posterior epithelium induce β-catenin nuclear accumulation in DBZ cells (red spots); yellow, *Jag1* positive zone; blue, *Notch1* positive zone; red arrows, nuclear β-catenin–Notch feedback loop; green arrows, nuclear-β-catenin–induced directional cell rearrangement; dashed lines, unknown mechanism.

The canonical Wnt pathway can activate directional cell motility during early stages of *Xenopus* gastrulation (34). Noncanonical Wnt/PCP members can control the axis of cell division orientation during long bone elongation (18) and can also mediate cell intercalation to achieve tissue/organ convergent extension (35, 36). Rho GTPases act downstream of the PCP pathway to reorganize the actin–NM network (24, 37, 38). Therefore, we had thought the PCP pathway should play an important role in feather polarizing activity. It turns out noncanonical Wnt/PCP pathway members are expressed later after long bud stage in feather development and do not function to orient feather buds.

Specifically localized cell proliferation may lead to asymmetric organ shape. Previous studies showed that asymmetric short bud stage cell proliferation is primarily localized to the posterior bud (4, 15). We found that this localized proliferation zone and DBZ colocalize only temporarily and have distinct spatial configurations later on. Thus, we consider it unlikely that the β-catenin/NM IIB module affects feather bud elongation through the direct regulation of localized proliferation. However, it is possible that both cell rearrangement and localized proliferation contribute to the bud elongation process.

NM II is a pivotal controller of cell migration and tissue architecture (21). It is critical for cell intercalation in *Drosophila* germ band convergent extension (20). NM IIB is the subtype most frequently reported to mediate directional cell migration in vertebrates (17, 39). In several cases canonical Wnt signaling lies upstream of NM II (40–42). In feather buds, anterior dermal cells (NM IIB-) remain relatively stationary whereas the posterior dermal cells (NM IIB+) exhibit polarized movements. Blocking NM IIB severely disrupted directional cell rearrangements and inhibited polarized organ elongation. Dual dye tracking experiments demonstrate that dermal cells can move horizontally, probably in a manner similar to cell intercalation in convergent extension. However, these data do not exclude the possibility that some cells also migrate vertically. If so, a chemoattractant likely is needed for directional guidance. *Shh* is known to be expressed in the distal bud epithelium starting from the asymmetric short bud stage, and serves as a directional cue.

Another important aspect of this work is the cross-talk between Wnt and Notch signaling in configuring the DBZ. A critical issue in tissue morphogenesis is how a signaling center can establish a cellular activity zone precisely and robustly. Morphogen gradients show fluctuations and even large variability between individuals (43). However, the zones for cell rearrangement (as seen here) and apoptosis (as used to generate space between barb branches) have well-defined domains. Thus, we need to know how noisy morphogen gradients are transformed into localized cell activity zones with sharp boundaries.

In our feather bud system we observed dramatic differences between the shape and fluctuation level of the Wnt gradient (noisy) and the Wnt response (relatively homogeneous with a sharp boundary). We also found nuclear β-catenin activates Notch signaling at the DBZ boundary. When we perturbed Notch signaling, the DBZ boundary destabilized, indicating the response to Wnt became noisy.

The morphogen gradient and threshold-based differentiation model (6) led us to ask how a noisy morphogen gradient is translated into well-defined cell domains. Several different mechanisms were previously proposed (7, 43). For our system we built a model to integrate Notch lateral inhibition and Wnt–Notch cross-talk. Mathematical simulations revealed the "denoising" and "ultrasensitizing" effects of Notch signaling that reshape the configuration of this localized polarized zone. The ultrasensitizing effect is crucial for the proper function of Wnt signaling as it is dictated by the fold change, rather than the absolute level of β-catenin (44). In other words a precipitous increase or decrease of nuclear β-catenin determines whether the downstream Wnt signaling effects are on or off. However, due to the positive feedback nature of the Wnt–Notch cross-talk, it alone cannot result in a steady state for nuclear β-catenin. One possibility is that the DBZ does not reach a steady state because its presence is temporal and the nuclear β-catenin positive cells are continuously moving. Another possibility is that an additional regulator may help to establish the steady state by counteracting Wnt activity. BMP is a candidate for this activity (45) (Fig. S7; *SI Model Details*).

The synergistic action of canonical Wnt and Notch signaling has been proposed to work as an integrated device, called the "Wntch" module (46). The cross-talk we observed in feathers is consistent with this concept: Wnt signaling activates a Notch ligand, such as *Jag1*. The Notch ligand stimulates neighboring cells to up-regulate Notch expression. This creates a positive feedback loop that maintains local Notch and Wnt signaling. Well-studied examples include establishing the *Drosophila* wing margin and size determination of the mouse otic placode (47, 48). It is possible the Wntch module can be coopted to function in different biological processes, and similar mechanisms may be adopted in regulating other localized activity zones.

Morphogenesis is achieved through patterned cell arrangements. This process is usually directed by biochemical signals (e.g., morphogen gradient), because chemical signals are pliable (e.g., the diffusion rate can be modified by extracellular matrix), adaptable (e.g., signal strength changes according to the location of signaling centers), and interactive (e.g., chemical signals can be synergistic or antagonistic). Frequently, a Turing model is cited as the driving force in pattern formation (49, 50). Physical forces also play key roles in shaping embryos (51). Chemical-based morphogenetic cues are prone to variations, whereas the physical activities that shape organs must be well-defined spatially. Hence, additional mechanisms are required to enhance the precision during this "chemical" to "physical" transition. Here we show that during feather bud elongation, the chemical based morphogenetic cue (Wnt7a gradient) is transformed into a relatively homogeneous and sharp-edged dermal zone enriched with nuclear β-catenin. This zone coincides with feather polarizing activity, which we defined using transplantation experiments. Through Notch-β-catenin feedback (core pathway) and Notch lateral inhibition

(modulatory pathway; Fig. 7), the Wnt gradient is converted to a threshold response, thus the sharp boundary of this localized polarizing zone. The nuclear β-catenin zone induces expression of NM IIB. The NM IIB-dependent cell rearrangement then drives the directional elongation of the whole feather bud.

The distinct morphogenetic process of our feather model helps reveal a polarity forming molecular module for oriented organ elongation. Similar morphogenetic processes may occur in many other organogenesis scenarios. We expect the fundamental principles we deciphered here will be applicable to organogenesis in general.

Methods

Charles River pathogen-free chicken embryos were staged (9) before use.

Section and Whole-Mount In Situ Hybridization. Probes: *cNotch1*, *cDelta1*, and *cSerrate1* (52). RCAS (53). *cHey1* probe was cloned using the following primers: Sense: AAGCTGGAGAAAGCCGAGAT; Antisense: TTTGCCAAGGTTTGCTGAT. The whole-mount and paraffin section in situ hybridization were done as described (54). Staining was visualized using either 5-bromo-4-chloro-3-indolyl-phosphate/nitro blue tetrazolium (blue) or Vector Red (red).

Section and Whole-Mount Immunostaining. Immunostaining antibodies: β-catenin (Sigma, 15b8 monoclonal for quantification; C-2206 for normal immunofluorescence); Wnt-7a (Abcam, ab100792); NM IIB (Hybridoma Bank, CMII 23); Phalloidin-FITC (Sigma,P-5282); proliferating cell nuclear antigen (PCNA, clone PC 10 DAKO); BrdU (Abcam, ab8955); smooth muscle actin (Sigma, A5228). RCAS (Hybridoma Bank, AMV-3C2); TUNEL kit (Roche applied science, 11684817910). Immunostaining follows our published method (54). Secondary antibody was Alexa Fluor 488 or Alexa Fluor 594 labeled.

Chromatin Immunoprecipitation. We used the protocol modified from R&D systems ExactaChIP β-catenin chromosome immunoprecipitation (ChIP) manual. The primers for PCR: WRE sense: GCTTGCACAACTTCCACTGA; WRE antisense: TGGAAGTGCAAAGTCTTGGA.

Short-Term BrdU Labeling. For short-term BrdU labeling (Sigma, catalog no. B5002), 10 μL of 1% BrdU was injected into the vein 4 h before embryo collection. The sample was then fixed in 4% paraformaldehyde overnight before further treatment.

Confocal Imaging. A Zeiss LS510 confocal microscope was used to image the fluorescently labeled specimens. Z-stack images were captured and processed in the Zeiss Laser Scanning Microscope Image Browser software.

Electroporation. Electroporation was performed as described (54). The embryo was exposed to three electric shocks at 16 V, 1 s interval between each shock (BTX ECM 830). Plasmids: RCAS-β-catenin was a gift of C. Tabin (Harvard University, Boston). RCAS-NICD, the chicken *Notch1* intracellular domain coding region, was inserted into Replication Competent Avian Sarcoma Virus Bryan Polymerase subtype Y destination vector using the Invitrogen Gateway system.

Skin Explant Culture and Drug/Bead Treatment, Transplantation of Different Parts of Feather Buds, and EMRR. Explant cultures were performed as described (55). Transplantation experiments: Part of unlabeled feather buds at symmetric short bud stage were removed from the explant and replaced with a region from a DiI- (3 mM) labeled explant (same stage). Drug treatment: the indicated concentrations of Blebbistatin, Y27632 or DAPT (Tocris) dissolved in DMSO were added to the explant culture media. Bead experiments: Affi-Gel Blue (Bio-rad) beads soaked with BSA (10mg/mL) or Wnt7a protein (PeproTech 120–31) were put on E7 dorsal dermis and cultured for 24 h. EMRR experiments were performed as described (11).

Cell Tracking on Skin Explant and Time-Course Imaging of Cell Behavior. Invitrogen Vybrant 5-Carboxyfluorescein Diacetate cell tracer (25 μM) was injected into anterior or posterior feather bud dermis at the late symmetric short bud stage and observed for 4 d. For dual dye tracking experiments, Invitrogen Qtracker 625 and Vybrant cell tracer were injected into two different spots at posterior bud mesenchyme and images were taken every 6 h.

In vitro cell culture: RCAS-β-catenin electroporated chicken embryo fibroblast cells were treated with 10 μM Blebbistatin or DMSO for controls. Cell movements were tracked with a Leica DFC300 FX camera.

Statistics. Paired sample *T* test, and independent two-sample *T* test and angular histogram plots were done with MATLAB 7. Statistics for Fig. 4*I* were calculated as follows: The movements of 25 cells picked randomly from each of 6 views were analyzed. "Severe direction change" is defined as a sudden change in direction between 45° and 135°, which is maintained for at least 100 μm.

Morphogen Gradient Measuring and Modeling. Wnt7a and β-catenin confocal images were analyzed with Fiji. A line (width = 50) was drawn from the posterior epithelial–mesenchymal boundary toward the center of the bud. Plot Profile recorded the signal intensity along this axis.

The influence from Wnt7a to DBZ is modeled using a Hill function, supported by the observation that there is the positive and reinforcing feedback loop from Lef-1 to Wnt7a (56). The Wnt–Notch cross-talk relationship was based on previous compartmental models (31). All simulations were performed using MATLAB (*SI Model Details*).

ACKNOWLEDGMENTS. We thank Dr. Plikus [Department of Developmental and Cell Biology, University of California, Irvine (UC Irvine)] for discussions. This research was supported by the National Institute of Arthritis and Musculoskeletal and Skin Diseases AR47364 (to C.-M.C. and R.W.), AR60306 (to C.-M.C. and T.-X.J.), AR 42177 (to C.-M.C.), GM67247 (to Q.N.), and National Science Foundation (NSF) Grants DMS-0917492 (to Q.N.) and DMS1161621. We acknowledge the Systems Biology course offered by UC Irvine Center for Complex Biology Systems P50GM76516 (Arthur Lander and Q.N.) for catalyzing model simulation of our experimental results. We thank the Cell and Tissue Imaging Core of the University of Southern California Research Center for Liver Disease (National Institutes of Health Grant P30 DK048522) for the use of the confocal microscope. The NM IIB antibody was obtained from the Developmental Studies Hybridoma Bank developed under the auspices of the National Institute of Child Health and Human Development and maintained by the Department of Biology, University of Iowa. A.L. is a predoctoral Fellow supported by a training grant from California Institute of Regenerative Medicine.

1. Slack JM (2008) Origin of stem cells in organogenesis. *Science* 322(5907):1498–1501.
2. Chuong CM, Randall VA, Widelitz RB, Wu P, Jiang TX (2012) Physiological regeneration of skin appendages and implications for regenerative medicine. *Physiology (Bethesda)* 27(2):61–72.
3. Wu P, Jiang TX, Suksaweang S, Widelitz RB, Chuong CM (2004) Molecular shaping of the beak. *Science* 305(5689):1465–1466.
4. Chodankar R, et al. (2003) Shift of localized growth zones contributes to skin appendage morphogenesis: Role of the Wnt/beta-catenin pathway. *J Invest Dermatol* 120(1):20–26.
5. Yu M, Wu P, Widelitz RB, Chuong CM (2002) The morphogenesis of feathers. *Nature* 420(6913):308–312.
6. Wolpert L, Tickle C (2011) *Principles of Development*, ed Tickle C (Oxford Univ Press, Oxford).
7. O'Connor MB, Umulis D, Othmer HG, Blair SS (2006) Shaping BMP morphogen gradients in the Drosophila embryo and pupal wing. *Development* 133(2):183–193.
8. Riddle RD, Johnson RL, Laufer E, Tabin C (1993) Sonic hedgehog mediates the polarizing activity of the ZPA. *Cell* 75(7):1401–1416.
9. Hamburger V, Hamilton HL (1951) A series of normal stages in the development of the chick embryo. *J Morphol* 88:49–92.
10. Noramly S, Morgan BA (1998) BMPs mediate lateral inhibition at successive stages in feather tract development. *Development* 125(19):3775–3787.
11. Chen CW, Jung HS, Jiang TX, Chuong CM (1997) Asymmetric expression of Notch/Delta/Serrate is associated with the anterior-posterior axis of feather buds. *Dev Biol* 188(1):181–187.
12. Viallet JP, et al. (1998) Chick Delta-1 gene expression and the formation of the feather primordia. *Mech Dev* 72(1-2):159–168.
13. Widelitz RB, et al. (1999) Wnt-7a in feather morphogenesis: Involvement of anterior-posterior asymmetry and proximal-distal elongation demonstrated with an in vitro reconstitution model. *Development* 126(12):2577–2587.
14. Noramly S, Freeman A, Morgan BA (1999) Beta-catenin signaling can initiate feather bud development. *Development* 126(16):3509–3521.
15. Desbiens X, Quéva C, Jaffredo T, Stéhelin D, Vandenbunder B (1991) The relationship between cell proliferation and the transcription of the nuclear oncogenes c-myc, c-myb and c-ets-1 during feather morphogenesis in the chick embryo. *Development* 111(3):699–713.
16. Chang CH, et al. (2004) Distinct Wnt members regulate the hierarchical morphogenesis of skin regions (spinal tract) and individual feathers. *Mech Dev* 121(2):157–171.
17. Rolo A, Skoglund P, Keller R (2009) Morphogenetic movements driving neural tube closure in Xenopus require myosin IIB. *Dev Biol* 327(2):327–338.
18. Li Y, Dudley AT (2009) Noncanonical frizzled signaling regulates cell polarity of growth plate chondrocytes. *Development* 136(7):1083–1092.
19. Zou H, Niswander L (1996) Requirement for BMP signaling in interdigital apoptosis and scale formation. *Science* 272(5262):738–741.

20. Kasza KE, Zallen JA (2011) Dynamics and regulation of contractile actin-myosin networks in morphogenesis. *Curr Opin Cell Biol* 23(1):30–38.
21. Vicente-Manzanares M, Ma X, Adelstein RS, Horwitz AR (2009) Non-muscle myosin II takes centre stage in cell adhesion and migration. *Nat Rev Mol Cell Biol* 10(11): 778–790.
22. Shanely RA, et al. (2009) IGF-I activates the mouse type IIb myosin heavy chain gene. *Am J Physiol Cell Physiol* 297(4):C1019–C1027.
23. Lo CM, et al. (2004) Nonmuscle myosin IIb is involved in the guidance of fibroblast migration. *Mol Biol Cell* 15(3):982–989.
24. Verdier V, Guang-Chao-Chen, Settleman J (2006) Rho-kinase regulates tissue morphogenesis via non-muscle myosin and LIM-kinase during Drosophila development. *BMC Dev Biol* 6:38.
25. Daudet N, Ariza-McNaughton L, Lewis J (2007) Notch signalling is needed to maintain, but not to initiate, the formation of prosensory patches in the chick inner ear. *Development* 134(12):2369–2378.
26. Tsao PN, et al. (2008) Gamma-secretase activation of notch signaling regulates the balance of proximal and distal fates in progenitor cells of the developing lung. *J Biol Chem* 283(43):29532–29544.
27. Caricasole A, et al. (2003) Functional characterization of WNT7A signaling in PC12 cells: Interaction with A FZD5 x LRP6 receptor complex and modulation by Dickkopf proteins. *J Biol Chem* 278(39):37024–37031.
28. Davis EK, Zou Y, Ghosh A (2008) Wnts acting through canonical and noncanonical signaling pathways exert opposite effects on hippocampal synapse formation. *Neural Dev* 3:32.
29. Wartlick O, Kicheva A, González-Gaitán M (2009) Morphogen gradient formation. *Cold Spring Harb Perspect Biol* 1(3):a001255.
30. Nakagawa O, et al. (2000) Members of the HRT family of basic helix-loop-helix proteins act as transcriptional repressors downstream of Notch signaling. *Proc Natl Acad Sci USA* 97(25):13655–13660.
31. Sprinzak D, et al. (2010) Cis-interactions between Notch and Delta generate mutually exclusive signalling states. *Nature* 465(7294):86–90.
32. Kiecker C, Niehrs C (2001) A morphogen gradient of Wnt/beta-catenin signalling regulates anteroposterior neural patterning in Xenopus. *Development* 128(21): 4189–4201.
33. Wang Y, Chang H, Nathans J (2010) When whorls collide: The development of hair patterns in frizzled 6 mutant mice. *Development* 137(23):4091–4099.
34. Brown JD, Hallagan SE, McGrew LL, Miller JR, Moon RT (2000) The maternal Xenopus beta-catenin signaling pathway, activated by frizzled homologs, induces goosecoid in a cell non-autonomous manner. *Dev Growth Differ* 42(4):347–357.
35. Goto T, Keller R (2002) The planar cell polarity gene strabismus regulates convergence and extension and neural fold closure in Xenopus. *Dev Biol* 247(1):165–181.
36. Heisenberg CP, et al. (2000) Silberblick/Wnt11 mediates convergent extension movements during zebrafish gastrulation. *Nature* 405(6782):76–81.
37. Tahinci E, Symes K (2003) Distinct functions of Rho and Rac are required for convergent extension during Xenopus gastrulation. *Dev Biol* 259(2):318–335.
38. Habas R, Kato Y, He X (2001) Wnt/Frizzled activation of Rho regulates vertebrate gastrulation and requires a novel Formin homology protein Daam1. *Cell* 107(7): 843–854.
39. Witze ES, Litman ES, Argast GM, Moon RT, Ahn NG (2008) Wnt5a control of cell polarity and directional movement by polarized redistribution of adhesion receptors. *Science* 320(5874):365–369.
40. Lee JY, et al. (2006) Wnt/Frizzled signaling controls C. elegans gastrulation by activating actomyosin contractility. *Curr Biol* 16(20):1986–1997.
41. Herman M (2001) C. elegans POP-1/TCF functions in a canonical Wnt pathway that controls cell migration and in a noncanonical Wnt pathway that controls cell polarity. *Development* 128(4):581–590.
42. Zimmerman SG, Thorpe LM, Medrano VR, Mallozzi CA, McCartney BM (2010) Apical constriction and invagination downstream of the canonical Wnt signaling pathway require Rho1 and Myosin II. *Dev Biol* 340(1):54–66.
43. Houchmandzadeh B, Wieschaus E, Leibler S (2002) Establishment of developmental precision and proportions in the early Drosophila embryo. *Nature* 415(6873):798–802.
44. Goentoro L, Kirschner MW (2009) Evidence that fold-change, and not absolute level, of beta-catenin dictates Wnt signaling. *Mol Cell* 36(5):872–884.
45. Kamiya N, et al. (2008) BMP signaling negatively regulates bone mass through sclerostin by inhibiting the canonical Wnt pathway. *Development* 135(22):3801–3811.
46. Hayward P, Kalmar T, Arias AM (2008) Wnt/Notch signalling and information processing during development. *Development* 135(3):411–424.
47. Zecca M, Struhl G (2007) Recruitment of cells into the Drosophila wing primordium by a feed-forward circuit of vestigial autoregulation. *Development* 134(16):3001–3010.
48. Jayasena CS, Ohyama T, Segil N, Groves AK (2008) Notch signaling augments the canonical Wnt pathway to specify the size of the otic placode. *Development* 135(13): 2251–2261.
49. Jung HS, et al. (1998) Local inhibitory action of BMPs and their relationships with activators in feather formation: Implications for periodic patterning. *Dev Biol* 196(1): 11–23.
50. Painter KJ, Hung GS, Wells KL, Johansson JA, Headon DJ (2012) Towards an integrated experimental–theoretical approach for assessing the mechanistic basis of hair and feather morphogenesis. *Interface Focus* 2:433–450.
51. Forgacs G, Newman SA (2005) *Biological Physics of the Developing Embryo* (Cambridge Univ Press, Cambridge, UK).
52. Myat A, Henrique D, Ish-Horowicz D, Lewis J (1996) A chick homologue of Serrate and its relationship with Notch and Delta homologues during central neurogenesis. *Dev Biol* 174(2):233–247.
53. Crowe R, Niswander L (1998) Disruption of scale development by Delta-1 misexpression. *Dev Biol* 195(1):70–74.
54. Jiang TX, Stott S, Widelitz RB, Chuong CM (1998) *Molecular Basis of Epithelial Appendage Morphogenesis*, ed Chuong CM (Landes Bioscience, Austin, TX), pp 359–408.
55. Ting-Berreth SA, Chuong CM (1996) Local delivery of TGF beta2 can substitute for placode epithelium to induce mesenchymal condensation during skin appendage morphogenesis. *Dev Biol* 179(2):347–359.
56. Jamieson C, Sharma M, Henderson BR (2011) Regulation of β-catenin nuclear dynamics by GSK-3β involves a LEF-1 positive feedback loop. *Traffic* 12(8):983–999.